

# **Physical control of phytoplankton distributions in the Alboran Sea: a numerical and satellite approach**

Elisa Garcia-Gorriz<sup>1</sup>, Mary-Elena Carr

Jet Propulsion Laboratory/Caltech, Pasadena, California

Short title: PHYSICAL CONTROL OF PHYTOPLANKTON IN ALBORAN

**Abstract.**

This study aims to identify the controlling processes of phytoplankton distributions in the Alboran Sea (western Mediterranean Sea). A three-dimensional primitive equations model, the Navy Layered Ocean Model, forced by satellite-measured winds from the European Remote Sensing satellites (ERS-1 and 2) and the NASA scatterometer (NSCAT), is used to examine circulation from January 96 to December 98 and to simulate the corresponding patterns of passive tracers within the basin. We discuss the impact of the basin circulation over the concurrent distributions of chlorophyll observed with the Sea-viewing Wide Field-of-view Sensor (SeaWiFS) and the Ocean Color and Temperature Scanner (OCTS). The upper layer is fertilized with nutrients which are transported by the western anticyclonic gyre from the coastal upwelling sites in the northwest. Nutrients are supplied also by eddy-induced upwelling in the periphery of the gyre path (estimated between 20 and 60% of that due to advection). Circulation controls the supply of nutrients and the primary production in the upper layer during the non-bloom months (late spring, summer, and early fall). During bloom regime, seasonal destratification is the dominant fertilizing process for the entire basin.

## 1. Introduction

The Alboran Sea is the western-most basin in the Mediterranean Sea, an evaporative semi-enclosed sea connected to the Atlantic Ocean by the Strait of Gibraltar (Fig. 1). A fresh and light Atlantic inflow ( $S < 36.5$  psu) penetrates the upper layer of the Alboran Sea with speeds of  $\sim 1 \text{ m s}^{-1}$ , while denser and saltier Mediterranean water ( $S > 38.4$  psu) outpours at depth at  $\sim 5 \text{ cm s}^{-1}$  into the Atlantic Ocean [Perkins and Saunders, 1984]. In its eastward progression into the Alboran Sea, the Atlantic influx generates a system of two quasi-permanent anticyclonic gyres (each approximately 100 km in diameter) which almost cover the entire basin. The gyres can normally be traced until depths of 200-250 m. The gyres can collapse, as is observed from satellite images below, though they re-appear. During its progression within Alboran, the Atlantic inflow mixes with the underlying water to produce the Modified Atlantic Water.

Two types of upwelling occur in different parts of the basin: wind-induced, mostly in the northern side of the western gyre (off the Spanish coast), and gyre-induced upwelling in the outskirts of the anticyclones. Although the western Mediterranean Sea is generally oligotrophic, high surface concentrations of pigments have been observed in Alboran [Morel and Andre, 1991; Arnone, 1995].

Since the 60s, the Alboran Sea circulation has been subject of many studies using *in situ* observations, laboratory experiments, and, more recently, satellite imagery and numerical models (see Speich et al. [1996] for a review of the different studies). The formation, persistence, mean position, intensity, and shape of this anticyclonic system are mainly determined by the coexistence and mixing of Atlantic and Mediterranean waters, variations in the mass flux through the Strait of Gibraltar, topography, the effect of the Earth's rotation, winds [Heburn and LaViolette, 1990], and generation of negative vorticity by vortex stretching [Speich et al., 1996].

In a previous paper about the Alboran Sea, we analyzed satellite-derived pigment and temperatures with a climatological perspective and proposed that the combined

effect of horizontal circulation, upwelling, and seasonal stratification controls the nutrient supply to the euphotic zone and leading to the pigment fields observed by ocean color satellites: Coastal Zone Color Scanner (CZCS), Ocean Color and Temperature Scanner (OCTS), and Sea-viewing Wide Field-of-view Sensor (SeaWiFS).

The present paper aims to examine the role of the circulation in phytoplankton distributions by using a 3-D primitive equation model forced by satellite-measured winds. The time domain of our study spans from November 1996 to February 1999, coinciding with the period of ocean color data availability, with a hiatus from July 97 (interruption of ADEOS operations) to September 97 (beginning of the SeaWiFS mission). Within this period, OCTS (November 96 to June 97), SeaWiFS (October 97 to February 99) chlorophyll-a patterns, satellite-measured sea surface temperatures (SST, November 96 to February 99), and velocity monthly fields are analyzed. In Alboran, nutrients and phytoplankton are transported by the anticyclonic circulation from the coastal upwelling sites in the north, as deduced from ocean color images. However, local biogeochemical processes also affect nutrient and pigment concentrations, especially in the outskirts of the gyre where eddy-induced upwelling occurs. We evaluate the 'in situ versus advective' contribution to these fields by introducing passive tracers into the circulation model and by using the sea surface temperatures computed with the model and a nitrate/temperature relationship derived from historical *in situ* data from the National Oceanographic Data Center (NODC)

This paper is organized as follows: section 2 describes the data sets examined and the circulation model, section 3 presents the results and discussion, and section 4 has the conclusions.

## 2. Data and Methodology

### 2.1. Data

We use the following satellite observations in this study: monthly phytoplankton fields (Chl hereafter) derived from OCTS (November 96 to June 97, resolution 9 km) and SeaWiFS (October 97 to February 99, 9 km), monthly SST distributions from the Pathfinder project (January 96 to August 98, 9 km) and from the MultiChannel Sea Surface Temperature (MCSST, October 97 to February 99, 19 km), and monthly wind fields measured by the NASA Scatterometer (NSCAT, November 96 to June 97,  $0.5^\circ$ ) and by the first and second European Remote Sensing satellites (ERS-1, January 95 to May 96), and ERS-2 (June 96 to February 99,  $1^\circ$ ).

To evaluate the role of nutrients we utilize *in situ* nitrate concentrations, temperatures, and salinities from the National Oceanographic Data Center (NODC).

### 2.2. The Circulation Model

We examine the dynamics of the Alboran Sea by using a three-dimensional primitive equations model, the Navy Layered Ocean Model (NLOM). The numerical simulations presented here are carried out using a 3-layer, finite-depth,  $\beta$ -plane, thermodynamic variant of NLOM for semi-enclosed seas. This circulation model is derived from Hurlburt and Thompson [1980] semi-implicit, layered, primitive equations model for the Gulf of Mexico. Over the intervening years the model has evolved and has been applied to a number of applications in various domains (Bering Sea, Caribbean Sea, Indian Ocean, Atlantic Ocean, and World Ocean), including the Alboran Sea [Preller, 1986] and the entire Mediterranean Sea [Heburn, 1995]. This layered model approach, based on isopycnal coordinates which are vertically integrated over the layer thickness, is a very efficient method to model the vertical structure of the open ocean.

A detailed description of the model equations and of different configurations can be

found in Preller [1986] and Heburn [1995]. Here, the three layers represent the thickness of the Atlantic Water (AW, 50 to 200 m), the underlying Levantine Intermediate Water (LIW, thickness 400 m), and the Mediterranean Deep Water (MDW, thickness is the depth of the basin minus the thickness of the overlying layers). The upper layer simulates the progression of the Atlantic influx within Alboran. The horizontal resolution is 10 km. ETOPO5 is used for the bathymetry grid. The salinity and temperature climatologies required at the start of the integration are from the Mediterranean Oceanographic Data Base (University of Liege, Belgium). The coefficient of eddy viscosity is  $100 \text{ m}^2 \text{ s}^{-2}$  and the grid interval Reynolds number  $Re > 20$ , ( $Re = v \Delta x / A$ , where  $v$  is the current,  $\Delta x$  is the grid spacing, and  $A$  is the eddy viscosity). As found by Preller [1986] and Heburn [1995], the simulated flow tends to be too viscous and suppresses flow instabilities observed in the ocean currents for Reynolds numbers less than approximately 20, while the simulations produce flows with numerically induced flow instabilities at  $Re > 100$ .

The circulation in the basin starts at rest with two open ports: an inflow port in the Strait of Gibraltar and an outflow port in the eastern border of the domain at longitude  $0^\circ$ . The Atlantic inflow enters the model domain through the narrow western port (20 km) representing the Strait of Gibraltar. The volume transport of Atlantic water has been evaluated between 0.9 and 2 Sv ( $1 \text{ Sv} = 10^6 \text{ m}^3 \text{ s}^{-1}$ ) [Bethoux, 1980; Kinder and Parrilla, 1984; Candela, 1991]. A transport of 1 Sv agrees with the results of numerical weather prediction models [Speich et al., 1996]. Other time-dependent inflow simulations specify a mean inflow transport of 0.9 Sv with amplitude variations of  $\pm 0.4$  Sv at a 14-day period [Heburn, 1995]. As this same author points out, the influence of inflow/outflow mass transport through the Strait of Gibraltar is a potential source of seasonal and interannual variability (in addition to wind variability) affecting the entire Mediterranean Sea. This issue has been debated largely in the past decades. The dominant source of flow variability through the Strait is tidal. We prescribe variable inflow values as follows, based on several numerical experiments. The incoming flow

through the Strait of Gibraltar is configured to 0.95 Sv in the upper layer, with an amplitude variation of  $\pm 0.2$  Sv over a 14 day period. The inflow angling is  $21^\circ$  to the northeast and changes sinusoidally [as in Preller, 1986] over a 183-day period (half a year). This inflow configuration is repeated for each year. This influx is compensated by the outflow through the eastern port (about 220 km wide). The inclusion of a moving lower layer resulted in only minor changes in the circulation, as also found by Preller [1986] with a 2-layer version of this model.

The model can be driven by atmospheric forcing; here, wind stresses computed from satellite-measured winds are used. The time domain for the model integration spans from January 95 to February 99. After several sensitivity analysis, an integration start at January 1995 resulted in the best circulation results for the time frame of our study, given by the availability of ocean color data: November 96 to February 99. The sequence of wind data used as forcing follows availability of satellite wind measurements: ERS-1 data from January 95 to September 96, ERS-2 from June 96 to October 96, NSCAT from September 96 to June 97, and ERS-2 from July 97 to February 99. NSCAT and ERS-1 and 2 data overlap within the NSCAT operation time. This fact gives a complete second sequence of wind measurements with only ERS-1 and 2 winds. Both cases of atmospheric forcing were run and the resulting currents varied only slightly.

When the Alboran island is not included, the gyre spreads westward beyond Cape Tres Forcas (at  $3^\circ\text{W}$  in the African coast) resulting in unrealistic circulation patterns. Thus, we configure a square of 1x1 grid points to represent the Alboran island (which is in fact slightly smaller than that), which serves to limit the eastern boundary of the western gyre.

We are interested in relatively long time periods, i. e. monthly time scales to describe the seasonal cycle. Although important, the effects of tides are not included. Our goal is to utilize the model results as a tool to understand the role of circulation in the monthly chlorophyll patterns in the Alboran Sea.

### 3. Results and Discussion

#### 3.1. Temporal progression of SST and phytoplankton pigments

The temporal evolution of the pigment concentration in the Alboran Sea presents two regimes throughout the year: the bloom regime from November to March (fall-to-winter), and the non-bloom, from May to September. Transition periods occur in April-May, when thermal stratification starts, and in October- November, coinciding with maximum wind variability and destratification within the basin. Since the bloom occurs at minimum PAR levels, light does not seem to be a limiting factor for phytoplankton growth in the Alboran basin throughout the year [Garcia-Gorriz and Carr, 1999]. This fall-to-winter bloom differs in timing from the annual blooms of other parts of the western Mediterranean Sea (such as the Gulf of Lions), where the main bloom occurs in spring with a secondary bloom in fall [Morel and Andre, 1991].

This temporal evolution in the Alboran basin is supported by the individual monthly phytoplankton distributions derived from the newest ocean color satellite sensors, SeaWiFS and OCTS. The scatterogram of monthly means of pigment versus temperature in Fig. 2 reveal this bloom/non- bloom progression with data to February 99). The two horizontal dashed lines in Fig. 2 approximately separate the bloom regime (for  $SST \leq 17.4^{\circ}C$ , from the no-bloom ( $SST \geq 19.5^{\circ}$ ). November (bloom) and May (non-bloom) values fall outside these temperature criteria. Though the average temperature is comparable for these months, the spatial pigment distributions are clearly distinct (not shown). Garcia-Gorriz and Carr [1999] defined a band of [pigment, SST] variability from all the values within western Alboran of CZCS-Chl and Pathfinder SST monthly climatologies, which illustrates the climatological progression of both variables. The band (also plotted in Fig. 2) is defined by a four-degree polynomial (fitted from CZCS-Chl vs. Pathfinder SST climatology maps) and extends  $\pm 1$  std ( $\pm 0.27$  mg/m<sup>3</sup>) of CZCS-Chl. The individual monthly points defined by OCTS or SeaWiFS versus

MCSST lie within the band, except for February and March 98 SeaWiFS values, which are slightly lower. These low values correspond to the poor bloom in the 97-98 winter. Autumn 97 was warmer than usual: October 97 maintained the summer SST values (warmer in 2°C with respect to climatological values, as seen in Fig. 2) and stratification, with weak winds (Fig. 3d and h). This situation produced a late destratification (and fertilization) of the basin and lower bloom pigment concentrations than normal. In contrast, October 98 had normal temperatures and winds (Fig. 4 d and g, and Fig. 2), and the 98-99 winter has phytoplankton concentrations consistent with the climatological scenario.

The comparison between the three different sensors (CZCS, SeaWiFS, and OCTS) is fraught with difficulty since they measure different wavelengths of irradiance and utilize different algorithms to estimate pigment concentration. However, the available values from these three ocean color data sets show that the SeaWiFS vs. MCSST and OCTS vs. MCSST values fall within the climatological band, thus supporting the CZCS-derived characterization of the annual evolution of pigment and temperature in the Alboran basin.

### **3.2. Velocity fields from the circulation model**

The monthly averages from either SeaWiFS, OCTS, or CZCS reveal that generally the highest Chl concentrations are located in the coastal areas of western Alboran (north and south coasts) and in the periphery of the western gyre (Fig. 3 or 4). The anticyclonic system (especially the western gyre) can be traced in most of the Chl and SST distributions in the same figures. During the bloom regime, high phytoplankton concentrations are observed throughout the Alboran basin. Coastal upwelling occurs predominantly in the northwest, off the Spanish coast. In June 97 and April and October 98, high Chl concentrations are observed in the north, corresponding to upwelling-favourable winds and coinciding in location with cold waters detected by SST

images (Fig. 3g, 4f, and g). The current fields computed with the circulation model for the first layer overlay the corresponding SST images. These velocities are comparable (though slightly smaller) to the Acoustic Doppler Current Profiler measurements in the upper layer in western Alboran [Garcia-Gorriz, 1995]. The velocity fields agree well with the circulation tracked thermally. Each SST image in Fig. 3 and 4 has an independent color-scale bar to enhance the visual contrast of the SST patterns.

From the 11-year climatology of SST, three thermal regimes are found in the basin [Garcia-Gorriz and Carr, 1999]. During the 'winter' regime (from November to April), surface Atlantic water in the vicinity of the Strait of Gibraltar is warmer than the water in Alboran and, therefore, the Atlantic inflow has a differentiated warm signature when progressing within the basin, as in January 97 and 98, and April 98 (Fig. 3a, 4a and b). For the 'transition' regime (May-June and October), the incoming inflow has similar SST to the water in west Alboran. Cold upwelled waters are detected in the northwest in June 97 and 98 (with strong upwelling-favourable winds in June 97) and are advected by the western gyre, which is unambiguously traced, both in SST and pigment images (Fig. 3c, g, and 4c, g). These June phytoplankton distributions are typical of the non-bloom period, except for the warmest time of the year. The situation during the 'summer' regime (from July to September) is reversed with respect to the 'winter' regime and the Atlantic inflow is colder. This is observed also in the anomalously warm October 97 (Fig. 3 d): the basin is stratified and only minor upwelling occurs in the north, as observed in the concurrent Chl distribution (Fig. 3h).

In October 97, the western gyre is not tracked clearly either from SST or phytoplankton distributions, and the simulated velocities show it to be compressed westward, almost collapsed (Fig. 3d and h). The same situation is observed in April 97, and the phytoplankton distribution seems to indicate collapse (Fig. 3b and f), in contrast with the situation in April 98 (Fig. 4b and f). In January 98, the compressed gyre is detected from the SST map, while the uniform (bloom) high concentrations

of pigments obscure flow patterns (Fig. 4a and e). The gyre was totally collapsed in February and March 98 as seen from SST, Chl, and simulated velocity distributions (Fig. 5a and b), and it reappeared in April 98 (Fig. 4b). As the numerical experiments by Preller [1986] indicated, when the inflow is not angled but due east, the Atlantic jet quickly turns to the south and forms a compressed smaller anticyclonic gyre (which may collapse) with the center shifted west and southward. This situation happens in cases where wind and pressure effects (and/or perhaps variations in the influx originated in the Atlantic Ocean) may minimize the inflow. Fig. 5a displays the model velocities considering the ERS-1 and 2 atmospheric forcing throughout the time span of the model run.

In most of the velocity fields resulting from the circulation model the Atlantic flow is primarily channeled between the Alboran island and the African coast in its eastward progression; a portion of this inflow turns west close to Cape Tres Forcas and recirculates, while the rest is deflected north and eastward. In the simulated velocities in June 97, we observe that the center of the western gyre is shifted northward and a portion of the inflow travels to the north of the island of Alboran (Fig. 3c). This deflection of a portion of the flow is consistent with the concurrent SST map, that shows an intrusion of cold water in east Alboran (also in Fig. 3). This flow pattern occurs occasionally according to Parrilla and Kinder [1984] and model results indicate that this type of change in the circulation can be caused by the sporadic increase of the northward directed transport [Preller, 1986]. In our case, the strong winds in June 97 seem to be responsible.

Although simulated currents generally agree well with the observed thermal patterns in western Alboran, the results from the model in the eastern side are less similar to the SST images (Fig. 3, 4, and 5). January 97, June 97, and March 98 provide the best agreement in eastern Alboran. Eastern Alboran is known to be more variable than the western basin and the eastern gyre can disappear for longer periods

of time [Viudez and Tintore, 1995]. The monthly averages computed from the model results may not reflect the actual flow patterns due to the high variability in the eastern part of the Alboran basin.

### 3.3. *In situ* and advective fertilization of the Alboran Sea

Nutrients and phytoplankton are transported in Alboran from the coastal upwelling sites in the north by the anticyclonic circulation throughout the year, as the velocity fields computed by the model indicate. This is more evident during non-bloom regime and transition months, when the chlorophyll-a distributions derived from satellite reveal high concentrations at the northwestern coast and in the periphery of the western gyre (Fig. 3 and 4.

However, *in situ* fertilization of the euphotic zone during the non-bloom period also occurs associated with eddy-induced upwelling in the periphery of the gyre. Maximum vertical velocities computed from the circulation model are observed in the northwest coast ( $10^{-4} \text{ m s}^{-1} \sim 10 \text{ m day}^{-1}$ ) coinciding in location with high concentrations of pigment, and close to the mouth of the Strait of Gibraltar. Fig. 6 shows the vertical velocity field in the upper layer for March 98, characterized by strong upwelling-favourable winds in the northwest (Fig. 4f). Upwelling also occurs in the eastern boundary of the western gyre (close to the Alboran island) but the velocities are smaller. Our model results in the northwestern Alboran are consistent with the vertical velocities inferred by Viudez et al. [1996] from potential vorticity conservation: about  $5 \text{ m day}^{-1}$  to the north of the western gyre, coinciding with cold (upwelled) waters detected by satellite imagery.

**3.3.1. Tracer simulations.** To simulate the advection of nutrients and/or phytoplankton, passive (dye-like) tracers are introduced into the circulation model. A concentration of tracer is released continuously (since time 0 in the model run) in the second layer. Five source locations (each within a box of  $1 \times 1$  grid points) in the

northwest Alboran coast (marked as triangles in Fig. 4e), from the Strait of Gibraltar eastward, are chosen to represent potential coastal upwelling sites within the area of maximum upwelling velocity common for most of the months. We then examine the tracer concentrations in the upper layer (i. e. distribution of the upwelled tracer).

As observed from the vertical velocities and pigment distributions, coastal upwelling occurs over a wide area. The tracer is advected by the current: it recirculates with the western gyre or it is transported to east Alboran. Fig. 4e, f, h, and g show the tracer concentration contours (thick lines correspond to high concentrations of tracer) overlaid on the SeaWiFS phytoplankton distributions. Maximum concentrations of advected tracer coincide horizontally with the highest values of pigments for April, June, and October 98, and they track the western gyre unambiguously (Fig. 4f, h, and g). In January 98 nutrients are also transported by the current but the bloom regime does not allow the tracking of the circulation by pigments (Fig. 4e).

Assuming a coastal source location closer to the Strait than the above mentioned sources, the tracer concentrations in the numerical experiments tend to accumulate towards the center of the anticyclonic circulation with the western gyre present. Both the inflow angle and the source location seem to condition this accumulation, As observed in March 98, with one source of tracer close to the Strait, the warm incoming Atlantic water accumulates to the southwest of the basin before traveling eastward (Fig. 5a and b). The western Alboran gyre is practically collapsed in March 98 and along the African coast the chlorophyll-a distribution is modified by circulation. This circulation scenario can be contrasted with that of April 98, when a fully developed western gyre is seen in model velocities, SST image and pigment distribution (Fig. 4b and f).

Besides advection from the coastal upwelling sites, seasonal destratification of the water column and local eddy-induced upwelling in the periphery of the gyre also fertilize the euphotic layer in Alboran [Garcia-Gorriz and Carr, 1999]. During the bloom regime, destratification seems to be the predominant process and affects the entire basin, as

observed for January 97 and 98 (Fig. 3e and 4e). During non-bloom, coastal and eddy-induced upwelled waters supply nutrients to support the phytoplankton biomass in the north coast and in the path of the western gyre, as observed in Fig. 4f, h, and g. According to Minas et al. [1991], the nitrate distribution is very homogeneous in the deep layers of the Alboran sea with a not very pronounced nitrate maximum. We can estimate the relative contribution of coastal and gyre-induced upwelled waters by comparing the tracer distributions for the above-mentioned 5 coastal sources and the tracer contributions of 5 sources on the gyre path (or gyre sources) close to the Alboran Island. The tracer concentration released continuously is the same (100 units  $\text{m}^{-3}$ ) for the 10 sources. Fig. 7 displays the concentration contours due to the coastal sources in June 98. The tracers are subsequently transported by the western gyre and concentrations of 130 units  $\text{m}^{-3}$  are found in the gyre. However, the resulting distribution for the gyre sources has maximum values of 80 in approximately the same locations (white contours in Fig. 7). For the time span of the numerical experiments, the eddy-induced contribution is 50-60% with respect to that advected from the coastal upwelling sites. In those months when coastal upwelling was significantly inhibited by stratification, as in October 97 (Fig. 3h), no apparent advection of nutrient-rich water was observed, except for some traces within the flow path close to the northwestern upwelling sites.

Though thermal stratification also affects in the eddy-induced upwelling, there is phytoplankton growth (though low) throughout the basin during the months of the strongest thermal stratification. For October 97, vertical velocities in the periphery of the gyre (not shown) correspond to upwelling ( $\sim 0.7 \text{ m day}^{-1}$ ). The observed absence of apparent transport of nutrient-rich waters from the coastal upwelling sites within the gyre path enable us to compare the satellite-derived Chl concentrations within the gyre path and with that occurred in the coastal upwelling sites at the time. The phytoplankton concentration within the area of the circulation path is about 20-30%

of the concentration present in the coastal upwelling sites (Fig. 3h). The simulated tracer concentration in the gyre path (due to gyre sources) for October 97, is 30-40% of the maximum concentrations found in the coastal sites. We believe that the difference between the 20-30% and the 30-40% is due to the fact that the tracer distributions simulated by the model do not consider the *in situ* processes of uptake (if simulating nutrients) or growth/mortality/grazing/sinking (if simulating phytoplankton), but rather estimate the availability of nutrient-rich waters both advected from coastal sites and upwelled by the gyre.

Subsequent to upwelling, the nutrient concentrations at the near-surface are determined by a competition between the residence time of the waters at the surface and phytoplankton uptake [Minster, 1989]. A volume of water traveling at velocity  $1 \text{ m s}^{-1}$  will reach the outflow port in the east in approximately 6 days (if it does not recirculate within the gyres) or 14 days (with one full recirculation in each gyre). Determining the biological time scales is difficult. Coastal chlorophyll levels in western Alboran can double within 24 hours, as observed by Arnone [1995] in October 1982. Considering that typical doubling rates are  $\sim 1$  day, the residence time of 6-14 days provides ample time to affect biomass.

The incoming Atlantic water may also constitute a source of nutrients for the Alboran Sea. Packard et al. [1988] proposed that nutrients are also supplied by nutrient-enriched Atlantic surface water that flows through the Strait and along the Spanish coast; this water is enriched from two separate sources: the first is by an injection of North Atlantic Central Water in the Gulf of Cadiz and the second source is the tidal mixing with deeper outflowing Mediterranean water at the Strait. Minas et al. [1991] proposed that this enriched Atlantic water curved along the Spanish coast as part of the gyre, supplementing the nutrient supply of upwelled waters on this coast which in turn enhanced primary production. This results were based on *in situ* measurements from October-November (and thus, at the beginning of the bloom

regime). We do not have nitrate measurements in the area and what we observed from the near-surface monthly images derived from OCTS and SeaWiFS is that the phytoplankton concentration at the mouth of the Strait (on the Alboran side) varies from the very low values in October 97 to higher values in October 98 (Fig. 3h and 4h). Likewise, values are low in March 98 but high in March 97 (Fig. 4f and 4f). The maximum values of pigments in March 97 are located in southwest Alboran, but although the observed Chl distribution could result from the nutrients carried by the Atlantic jet (with the gyre collapsed), it is more likely to interpret it as caused by the upwelling-favourable winds in the African coast. Moreover, for some of the bloom months the pattern of pigments indicates that the Atlantic inflow presents low pigment concentrations in comparison with the surrounding waters in Alboran. This is the case of January 99, where the low pigment tongue from the Strait seems to trace the incoming Atlantic water (Fig. 8). In fact, from the corresponding SST image (not shown) the warm Atlantic inflow is accumulated towards the southwest coast, and the velocities from the model indicate that center of the western gyre is shifted southwestward, agreeing with the concurrent thermal pattern. In conclusion, monthly pigment distributions throughout the year do not reflect a steady nutrient-rich Atlantic inflow fertilizing Alboran.

In January 99 (during bloom regime), the strong winds in the northeast favour the occurrence of coastal upwelling, inducing phytoplankton growth (Fig. 8). This coastal upwelling situation contrasts with January 97 and 98 (both with weak winds), when pigment images did not inform about the occurrence of upwelling and only numerical simulations indicated its presence (Fig. 3e and 4e).

**3.3.2. Nitrate concentrations, distribution residual, and primary production.** To evaluate the effect of the advective distribution, we use the tracer results and the satellite-derived pigment distributions to compute a variable we call residual. The residual is the difference between normalized satellite-derived pigments

and normalized tracer concentrations of the tracer field (from the 5 coastal tracers mentioned above). By subtracting the advective contribution from the normalized chlorophyll distribution, we assess the relative roles of passive transport and *in situ* net growth, which includes the source term (phytoplankton growth) and the loss terms (sinking + grazing + mortality). Where negative values of residual are found, the net transport is higher than net growth. This mainly occurs within the path of the anticyclonic jet, as observed in Fig. 9c to f. Net growth is higher than transport for positive values of the residual, which are mainly detected in the periphery of the western gyre and in the northeast of the basin (Fig. 9c to f). Simulated nitrate concentration (only available when and where temperatures  $< 17^{\circ}\text{C}$ ) explains 67% of the variance of the residual. Growth occurs where there is nitrate.

Another approach to simulate the concentration of nutrients in Alboran uses the upper layer temperatures computed with the model and a linear nitrate-temperature relationship derived from historical NODC *in situ* measurements for the upper 60 m of the water column. By the linear fit, zero nitrate concentration occurs at  $17.5^{\circ}\text{C}$  and we set nitrate to zero for temperatures  $> 17.5^{\circ}\text{C}$  to avoid negative values of nitrate concentration. For this reason, June and October 98 have a null field of simulated nitrate in the sequence of nitrate distributions shown in Fig. 9. In winter and early spring, the maximum concentrations of simulated nitrate are found in the north and east of the basin, as seen for January and April 98 (Fig. 9i and j). Compared to the phytoplankton distributions in Fig. 4, pigments are observed throughout Alboran in January 98 and high values of nitrate coincide approximately in location with high values of chlorophyll. However, in February and March 98 high values of nitrate (not shown) correspond to low values of pigments (Fig. 5b for March 98). It seems that there is an important source term of nitrate that we are not including within this estimate, the advective contribution.

Finally, we estimate the primary production in the upper-layer within the Alboran

basin by using the algorithm developed by Howard and Yoder [1997]. This algorithm uses phytoplankton observations, mixed layer depth, SST, and Photosynthetic Active Radiation (PAR) values. Here we use satellite-derived pigments from OCTS and SeaWiFS, the first layer temperatures from the circulation model, an 8-year climatology of PAR [Bishop et al., 1997], and the depth of the first layer from the circulation model. A surprising result was that the primary production during the bloom regime (e.g. January 98, Fig. 9g) is low compared to non-bloom or transition months (Fig. 9h to j). This results from the lower PAR values in winter. Sensitivity experiments applied on the primary production model in the Alboran Sea show that if we consider a constant PAR input (the average PAR in Alboran throughout the year,  $80 \text{ W m}^{-2}$ ), the bloom regime months have high primary production. For the Alboran Sea, where light availability does not seem to be a limiting factor for the phytoplankton growth throughout the year [Garcia-Gorriz and Carr, 1999], the algorithm by Howard and Yoder [1997] seems to be underestimating the primary production during the bloom regime. During the non- bloom regime (that is, in late spring, summer, and early fall), high values of primary production correspond to the northwestern upwelling sites and the anticyclonic circulation pattern. The western gyre is traced from primary production distributions in March, June, and October 98 (Fig. 9h to j). We observe that there is almost an order of magnitude of difference between the maximum values of primary production ( $\sim 2.5 \text{ g m}^{-2} \text{ day}^{-1}$  of C) and the rest of the basin.

#### 4. Conclusions

- 1) The upper layer velocity fields computed with a circulation model, which is forced with satellite-measured winds and a prescribed variable inflow, agree well with the progression of Atlantic waters tracked with SST and phytoplankton distributions within the Alboran basin for the time span considered. The horizontal pattern of the current field agrees better in western than in eastern Alboran. Specific characteristics

of the circulation which are observed from the SST (and some pigment) images are successfully reflected in the simulated currents: the temporary collapse of the western gyre in March 98 (Fig. 5) and the shifting of a portion of inflow north of the island of Alboran in June 97 (Fig. 3c)

2) During the bloom regime, the fertilization of the photic zone throughout Alboran is principally due to the destratification of the water column. At any time throughout the year and specially during non-bloom, circulation has a dominant role in fertilizing the basin by advecting nutrient and/or phytoplankton-rich waters from the northwestern coastal upwelling sites. The incoming Atlantic water does not seem to be a steady fertilizer of the Alboran basin.

3) For the time domain of the numerical experiments, the eddy-induced upwelling of tracer is estimated between 20 and 60% of that advected from the coastal upwelling sites. When we compared the tracer and pigment concentrations during the time when coastal upwelling is significantly inhibited by stratification and no apparent advection of nutrient-rich water is occurring, the tracer values due to gyre sources represent a 30-40% of the concentration at the coastal sites, while the phytoplankton maps indicate only a 20-30%. This discrepancy is probably due to the fact that the tracer distributions we obtained do not consider uptake (if representing nutrients) or growth/mortality/grazing/sinking (if representing algae). Nevertheless, they provide a valuable estimate of the relative availability of nutrient-rich waters for phytoplankton growth.

4) Primary production computed with Howard and Yoder [1997] algorithm traces the anticyclonic circulation in the upper layer of the Alboran basin during late spring, summer, and early fall (non-bloom regime). Maximum values correspond to the northwestern upwelling sites and the western gyre path. There is almost an order of magnitude of difference between the maximum values of primary production ( $\sim 2.5 \text{ g m}^{-2} \text{ day}^{-1}$  of C) in the gyre and northwest and the rest of the basin. Primary

production during bloom months seem to be underestimated by the primary production algorithm.

**Acknowledgments.** The authors thank Tammy Townsend (Stennis Space Center, Naval Research Laboratory) for providing the NLOM code. Her knowledgeable help was fundamental to adapt the CRAY code to the Alboran Sea and to run it successfully. We also thank W. Tim Liu and Wenqing Tang (both at JPL/Caltech) for providing the NSCAT data, the Goddard DAAC for the SeaWiFS and CZCS data sets, CERSAT (IFREMER, France) for the ERS-1 and 2 data sets, the NOAA/NASA AVHRR Pathfinder project for daily sea-surface temperature via JPL-PODAAC, who also provided the MCSST data, and MODB (Univ. of Liege, Belgium) for the temperature and salinity climatologies. The National Space Development Agency of Japan (NASDA) retains ownership of the OCTS (ADEOS) data. NASDA supports the authors in acquiring the satellite data at a marginal cost. The research in this paper was carried out in the Jet Propulsion Laboratory/California Institute of Technology under a contract with NASA. E. G.-G. is funded by the National Research Council and E.G.-G. and M.-E. C., by the NASA Ocean Biogeochemistry Program.

## References

- Arnone, R. A., The temporal and spatial variability of Chlorophyll in the western Mediterranean. Coastal and Estuarine Studies in *Seasonal and Interannual Variability of the Western Mediterranean Sea*, edited by P.E. LaViolette, pp. 195-225, AGU, 1995.
- Bethoux, J. P, Mean water fluxes across sections in the Mediterranean Sea, evaluated on the basis of water and salt budgets and of observed salinities , *Oceanol. Acta*, 3, 79-88, 1980.
- Bishop J. K. B., W. B. Rossow, E. G. Dutton, Surface solar irradiance from the International Satellite Cloud Climatology Project 1983-1991, *J. Geophys. Res.- Atmospheres*, 102(6), 6883-6910, 1997.
- Candela, J., The Gibraltar Strait and its role in the dynamics of the Mediterranean Sea, *Dyn. Atmos. Oceans*, 15, 2267-2991, 1991.
- Garcia-Gorriz, E., Aplicacion de un Perfilador Acustico por Efecto Doppler a la medida de corrientes marinas en el Mediterraneo Occidental, *Ph. D. Thesis*, Universitat Politecnica de Catalunya, Barcelona (Spain), 1995.
- Garcia-Gorriz and E., M.- E. Carr, The climatological annual cycle of satellite- derived phytoplankton pigments in the Alboran Sea, *Geophys. Res. Lett.*, in press, 1999.
- Heburn, G. W., The Dynamics of the Seasonal Variability of the Western Mediterranean Circulation in *Seasonal and Interannual Variability of the Western Mediterranean Sea*, edited by P.E. LaViolette, pp. 249-285, AGU, 1995.
- Heburn, G. W. and P. E. LaViolette, Variations in the structure of the anticyclonic gyres found in the Alboran Sea, *J. Geophys. Res.*, 95(2), 1599-1613, 1990.
- Howard, K. L., J. A. Yoder, Contribution of the Subtropical Oceans to Global Primary Production in *Space Remote Sensing of subtropical Oceans*, edited by C.- T. Liu, *COSPAR Colloquia Series*, volume 8, pp. 157-168, Pergamon, 1997.
- Hurlburt, H.E., J. D. Thompson, A Numerical Study of Loop Current Intrusions and Eddy Shedding, *J. Phys. Oceanogr.*, 10(10), 1611-1651, 1980.

- Kinder, T. H., G. Parrilla, Shallow hydrographic structure in the western Alboran Sea, October 1982, in *Donde va? Meeting Report*, edited by G. Parrilla, Instituto Español de Oceanografía, 1995.
- Minas, H. J., B. Coste, P. LeCorre, M. Minas, P. Raimbault, Biological and geochemical signatures associated with the water circulation through the Strait of Gibraltar and in the western Alboran Sea, *J. Geophys. Res.*, *96*(5), 8755-8771, 1991.
- Minster, J.-F., Introduction to chemical tracers of the ocean circulation in *Oceanic Circulation Models: Combining Data and Dynamics - NATO ASI Series*, edited by D. L. T. Anderson & J. Willebrand, pp. 345-376, Kluwer Academic Publishers, 1989.
- Morel, A. and J.-M. Andre, Pigment distribution and primary production in the western Mediterranean as derived and modeled from Coastal Zone Color Scanner observations, *J. Geophys. Res.*, *96*(7), 12685-12698, 1991.
- Packard, T. T., H. J. Minas, B. Coste, R. Martinez, M. C. Bonin, J. Gostan, P. Garfield, J. Christensen, Q. Dortch, M. Minas, G. Copin-Montegut, C. Copin-Montegut, Formation of the Alboran oxygen minimum zone, *Deep-Sea Res.* *35*(7), 1111-1118, 1988.
- Parrilla, G., T. H. Kinder, The physical oceanography of the Alboran Sea. In *Proceedings of NATO advanced Research Group workshop*, edited by H. Charnock, La Spezia, 1984.
- Perkins, H., K. D. Saunders, Sections of current, salinity and temperature in the northwestern Alboran Sea, October 1982 in *Donde va? Meeting Report*, edited by G. Parrilla, Instituto Español de Oceanografía, 1995.
- Preller, R. H., A Numerical Model Study of the Alboran Sea Gyre, *Prog. Oceanog.*, *16*, 113-146, 1986.
- Speich, S., G. Madec, M. Crepon, A strait outflow circulation process study: the case of the Alboran Sea, *J. Phys. Oceanogr.*, *26*, 320-340, 1996.
- Viudez, A., J. Tintore, Time and space variability in the eastern Alboran Sea in March- May 1990, *J. Geophys. Res.*, *100*(8), 8571-8586, 1995.

Viudez, A., J. Tintore, R. L. Haney, Circulation in the Alboran Sea as determined by quasi-synoptic hydrographic observations. Part I: three-dimensional structure of the two anticyclonic gyres, *J. Phys. Oceanogr.*, **26**, 684-705, 1996.

---

E. Garcia-Gorriz and M.-E. Carr, Jet Propulsion Laboratory/Caltech, MS 300/323, 4800 Oak Grove Dr., Pasadena, CA 91109. (e-mail: eg@pacific.jpl.nasa.gov)

Received \_\_\_\_\_

---

<sup>1</sup>Now at the Institut de Ciencies del Mar- CSIC, Barcelona, Spain.

**Figure 1.** Geographical location of the Alboran basin (limited by dashed line) within the western Mediterranean Sea

**Figure 2.** Scatterogram of pigment concentration and sea surface temperature for [SeaWiFS-Chl, MCSST] (black), [CZCS-Chl, Pathfinder SST] (dark gray), and [OCTS-Chl, MCSST] (light gray) in the western gyre region. The numbers in the plot indicate the corresponding month and year for SeaWiFS and OCTS, while the month of the year for climatological CZCS.

**Figure 3.** a) to d) Monthly distributions of Pathfinder SST for January, April, June, and October 1997. June 97 is shown in steady of July (and the every third month sequence broken) because no OCTS data was available. The SST images are overlapped by the first layer currents resulting from the circulation model (white arrows). These currents were forced with the ERS-1&2/NSCAT sequence. The Alboran island blue patch is provided by the SST data sets. e) to h) Same months for phytoplankton concentrations (from OCTS or SeaWiFS). They are overlapped by the available satellite-measured winds (NSCAT or ERS-2).

**Figure 4.** Same as in Fig. 3 but for 1998.

**Figure 5.** Same as in Fig. 3 but for March 98. The currents are forced with the ERS-1&2 sequence.

**Figure 6.** Contours of vertical velocities for March 98

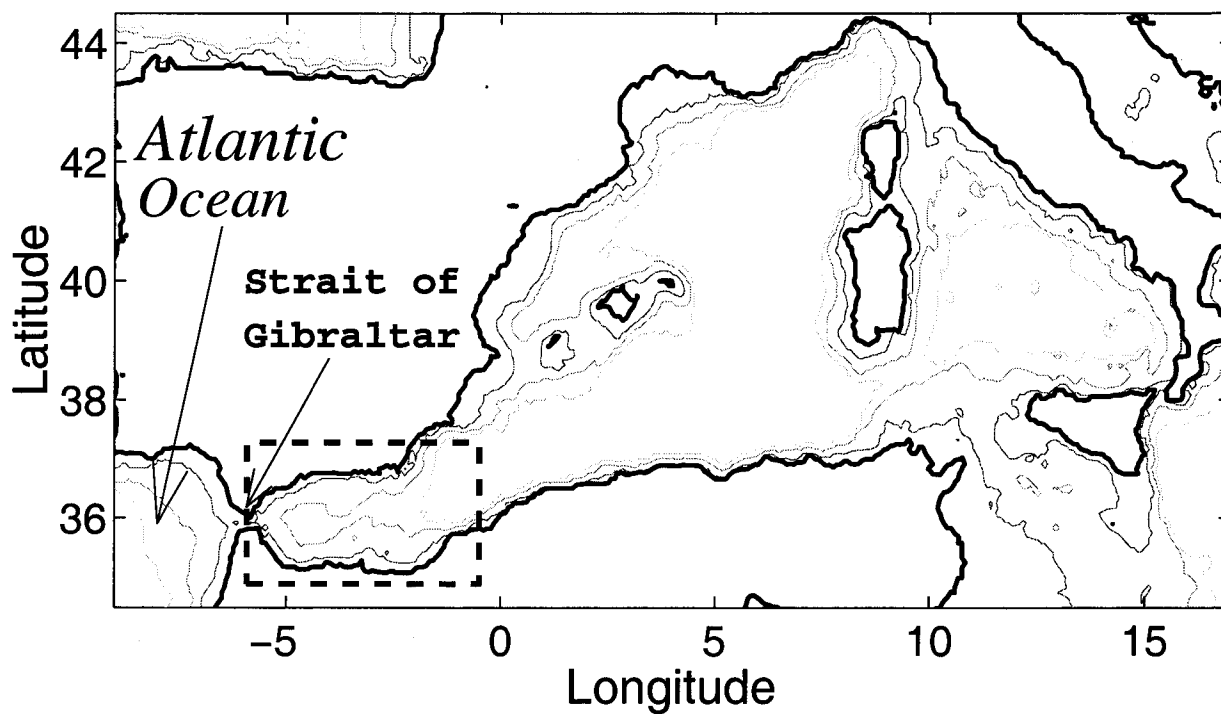
**Figure 7.** Concentration contours of passive tracer in June 98 due to five coastal sources (black lines and scale of gray) and five gyre sources on the gyre path close to the Alboran Island (white lines)

**Figure 8.** SeaWiFS phytoplankton distribution in January 99 with ERS-2 winds overlapped.

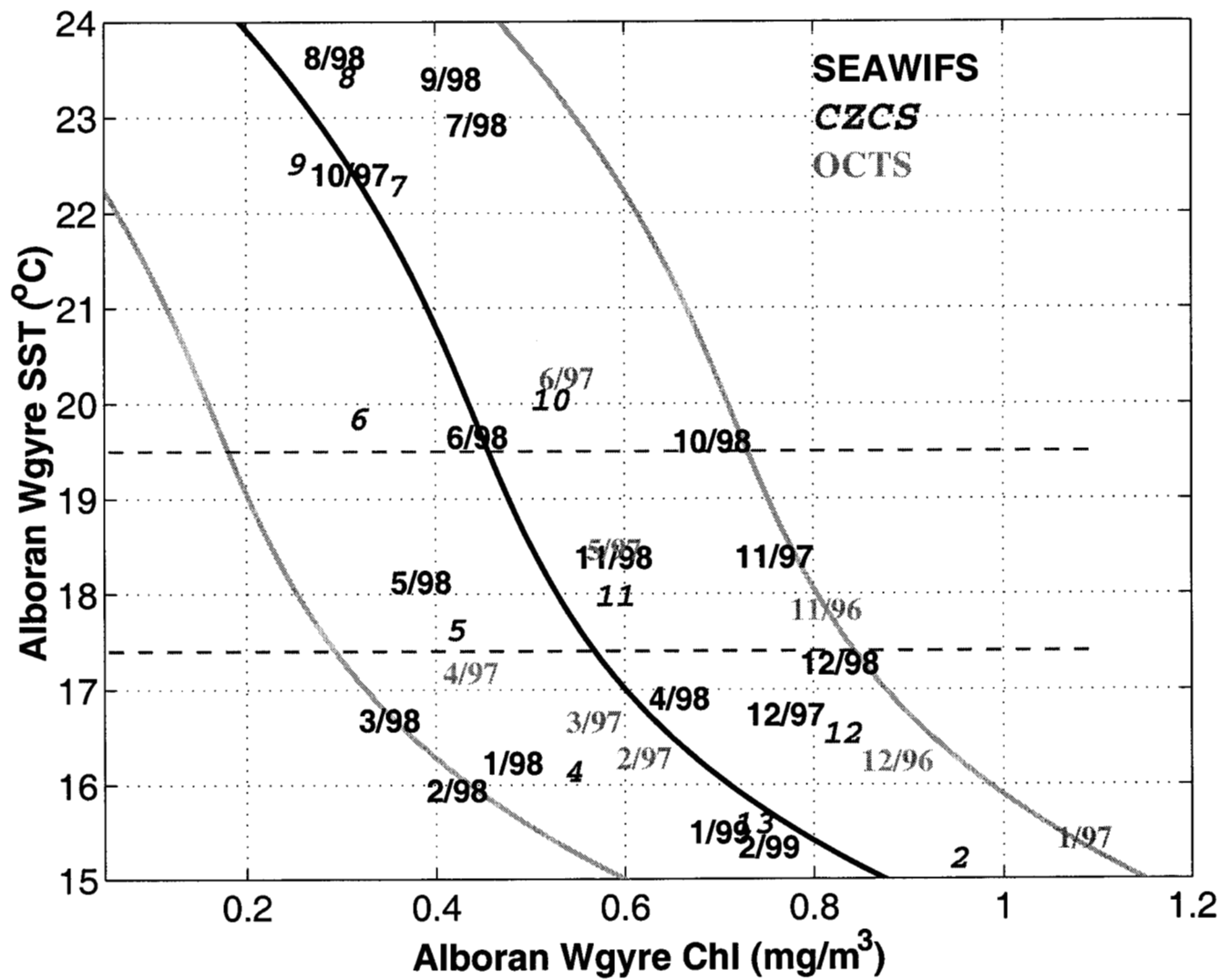
**Figure 9.** a) and b) Simulated nitrate distributions for ( $\text{mg m}^{-3}$ ) January and March 98. c) to f) Residual distributions ( $\text{mg m}^{-3}$ ) for January, March, June, and October 98. g) to j) Primary production ( $\text{g C m}^{-2} \text{ day}^{-1}$ ) for the same months.

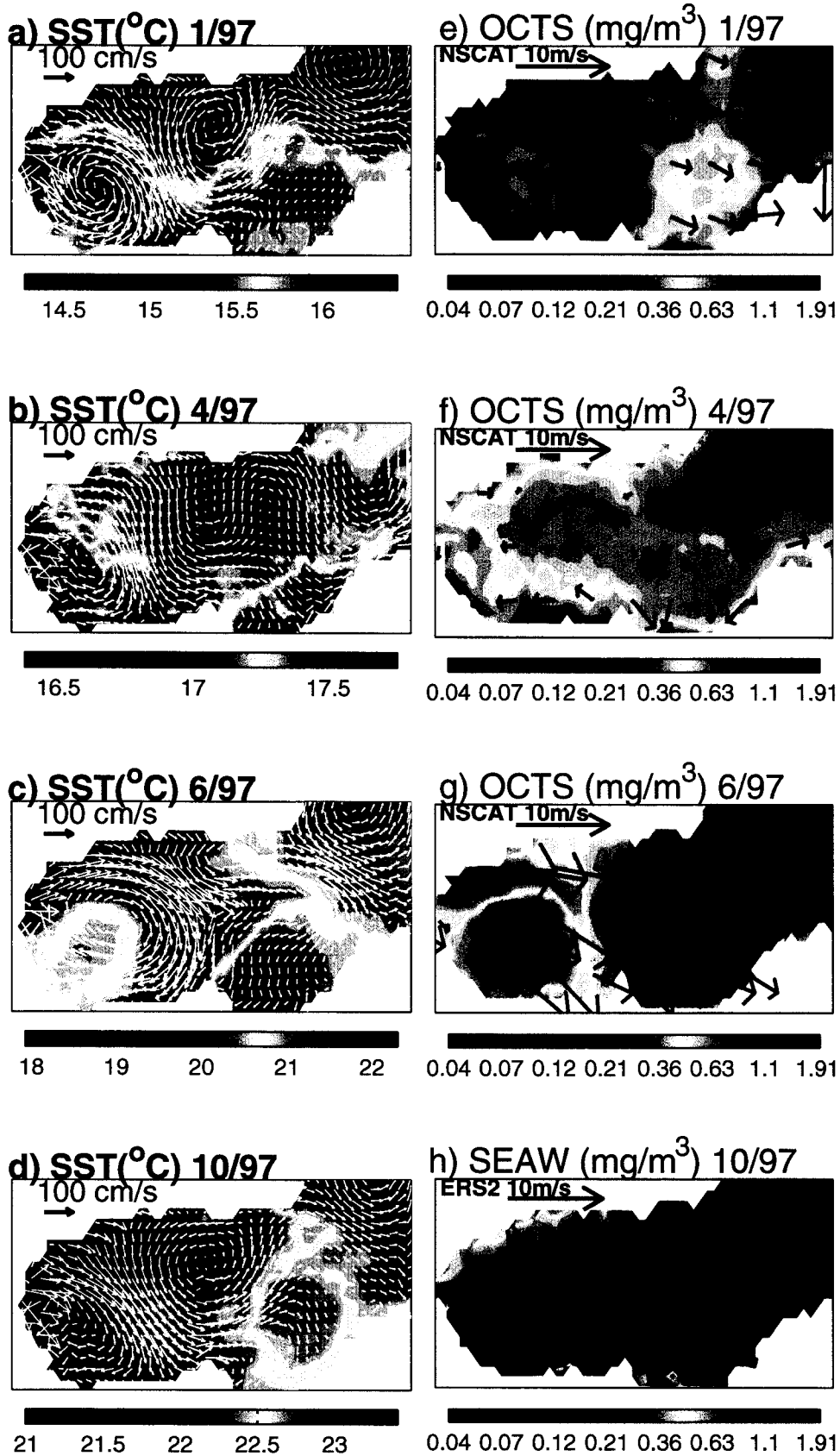
**FIGURE 1**

**Western Mediterranean Sea**

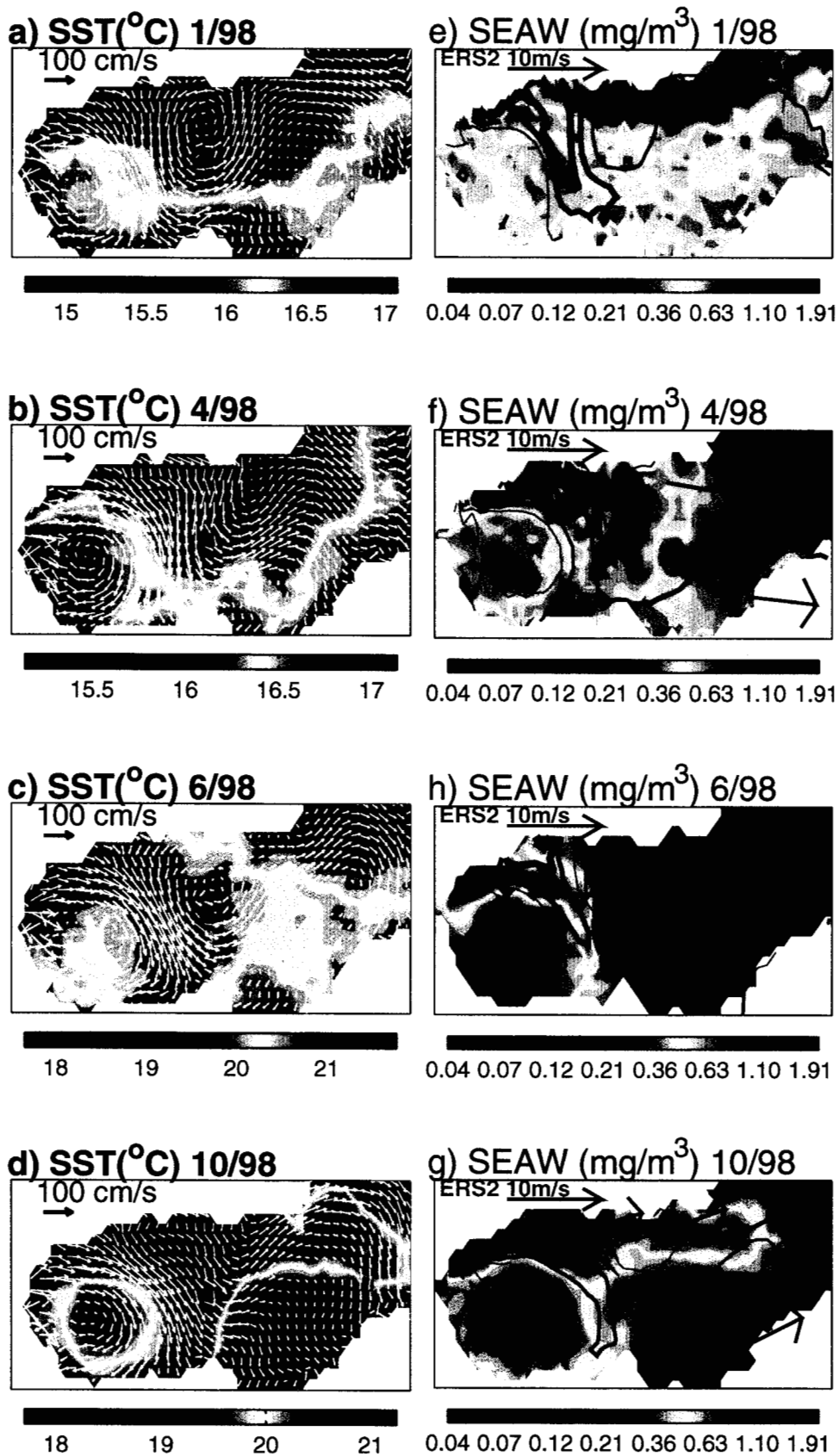


**FIGURE 2**

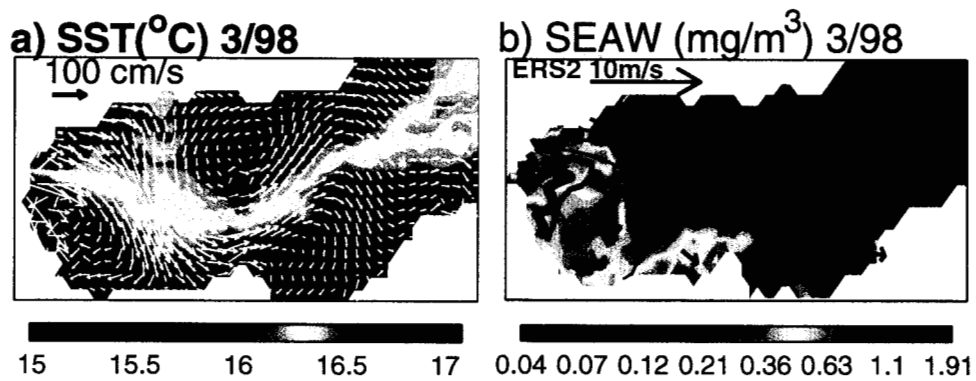




**FIGURE 3**



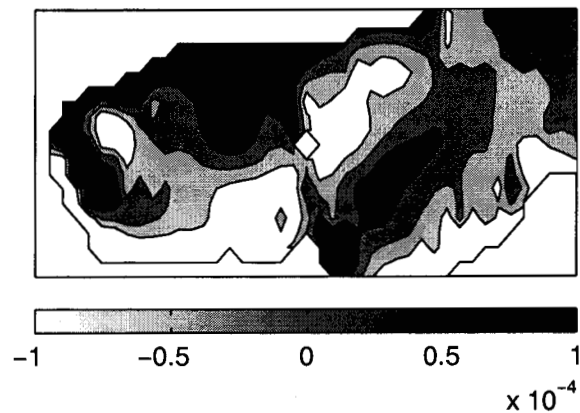
**FIGURE 4**



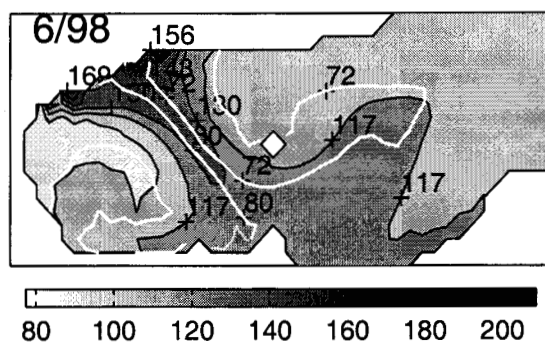
**FIGURE 5**

**FIGURE 6**

VERT VEL (m/s) 4/98

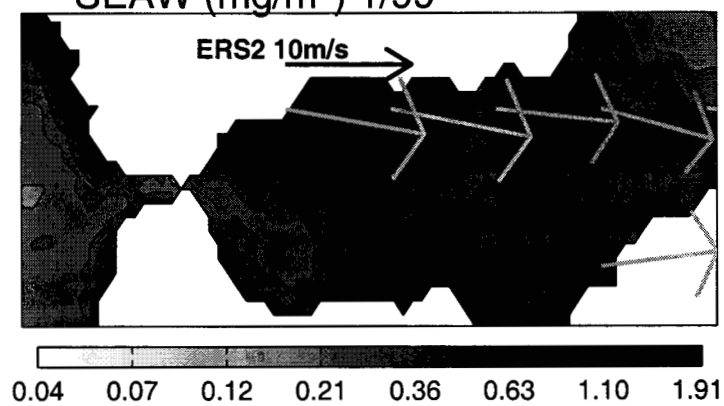


**FIGURE 7**



**FIGURE 8**

SEAW ( $\text{mg}/\text{m}^3$ ) 1/99



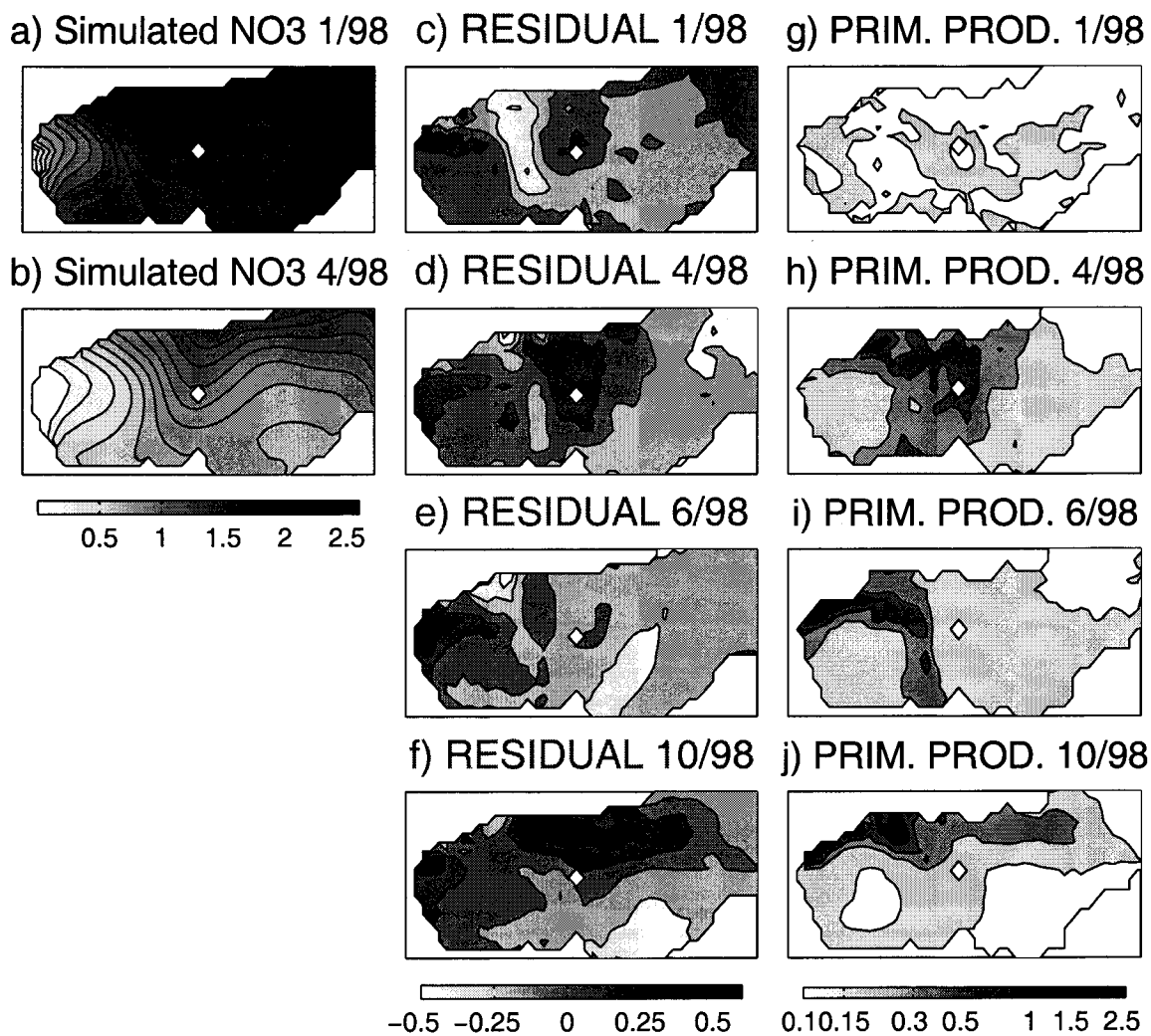


**FIGURE 9**